

From molecules to scaffolds to functional groups: building context-dependent molecular representation via multi-channel learning

Yue Wan¹, Jialu Wu², Tingjun Hou^{2*}, Chang-Yu Hsieh^{2*}, Xiaowei Jia^{1*}

University of Pittsburgh, Computer Science Department, Pittsburgh, PA 15260, United States¹

*Innovation Institute for Artificial Intelligence in Medicine of Zhejiang University,
College of Pharmaceutical Sciences, Zhejiang University, Hangzhou, 310058, China²*

Abstract

Reliable molecular property prediction is essential for various scientific endeavors and industrial applications, such as drug discovery. However, the scarcity of data, combined with the highly non-linear causal relationships between physicochemical and biological properties and conventional molecular featurization schemes, complicates the development of robust molecular machine learning models. Self-supervised learning (SSL) has emerged as a popular solution, utilizing large-scale, unannotated molecular data to learn a foundational representation of chemical space that might be advantageous for downstream tasks. Yet, existing molecular SSL methods largely overlook domain-specific knowledge, such as molecular similarity and scaffold importance, as well as the context of the target application when operating over the large chemical space. This paper introduces a novel learning framework that leverages the knowledge of structural hierarchies within molecular structures, embeds them through separate pre-training tasks over distinct channels, and employs a task-specific channel selection to compose a context-dependent representation. Our approach demonstrates competitive performance across various molecular property benchmarks and establishes some state-of-the-art results. It further offers unprecedented advantages in particularly challenging yet ubiquitous scenarios like activity cliffs with enhanced robustness and generalizability compared to other baselines.

1 Introduction

Empowered by the advancement of machine learning techniques, molecular machine learning has shown its great potential in computational chemistry and drug discovery [16, 29]. The data-driven protocol allows the model to infer biochemical behaviors from simple representations like SMILES sequence [44] and molecular graph, enabling fast identification of drug candidates via rapid screening of vast chemical spaces [15], as well as prediction of binding affinity, toxicity, and other pharmacological properties [46, 40]. These advancements significantly accelerate the drug discovery procedures, saving time and efforts from the traditional wet-lab experiments [17, 11]. However, it is fundamentally challenging to learn an effective and robust molecular representation via machine learning, limited by the expensive gathering of precise biochemical labels and the complexity underlying the structure-property relationships (SPR). With limited molecule data, models may become overly adapted to specific structural patterns within the training molecules, making it fail to generalize to the broader chemical space. In addition, the challenge of “activity cliffs” (AC) [26] in drug discovery, where minor changes in molecular structure significantly alter the biological activity, further impose obstacles in developing accurate Quantitative SPR (QSPR) models [40, 35, 32, 9].

Inspired by the success of the pretrain-finetune workflow in computer vision [8] and natural language processing [10, 28], various methods in molecule self-supervised learning (SSL) [18, 30, 47, 42, 50, 21, 13, 12] have emerged. In the self-supervised setting, machine learning models are pre-trained to learn generic

*Corresponding authors.

E-mail addresses: tingjunhou@zju.edu.cn (T. Hou), kimhsieh@zju.edu.cn (C.-Y. Hsieh), xiaowei@pitt.edu (X. Jia)

molecule representations by optimizing the performance on pre-defined pre-training tasks on large-scale unannotated molecule data. These tasks are designed in a way such that solving them requires identification of important structural patterns and understanding of rudimentary chemical knowledge. Existing molecule SSL methods can be mainly classified into two categories: predictive and contrastive. Predictive learning [18, 22, 30, 47] aims to predict structural components given contexts at different levels, which mainly focuses on *intra-data* relationship. Hu et al. [18] conduct masked attribute prediction, where the model is pre-trained to predict the masked atom/bond attribute (e.g., atom type, bond direction). MoleBERT [47] further improves masked attribute prediction into masked atom prediction. GROVER [30] attempts to predict the masked substructure. Besides, it also proposes motif prediction, where the existence of functional groups are predicted as a multi-label classification task. These two tasks are often framed as molecule context prediction. Contrastive learning [55, 41, 48, 53, 47, 50, 21], initially proposed in computer vision [6], aims to learn the *inter-data* relationship by pulling semantic-similar data samples closer and pushing semantic-dissimilar samples apart in the representation space. Note that this idea aligns well with common heuristics in chemistry, where structurally similar molecules are likely to exhibit similar physicochemical and biological properties. Most works attempt to generalize the same SSL methods across multiple graphical domains (e.g., social networks and molecular graphs), whereas it is unsure whether the same learning schemes are compatible to all settings. Recently, several studies have pointed out that the generalized SSL methods may fail to learn effective molecular representation. RePRA [54] was proposed as a metric for measuring the representations’ potential in solving activity cliffs and scaffold hopping [5], and experiments showed that most SSL pretrained representations perform worse than the molecule fingerprint. The work in [36] explored various graph SSL methods on molecule and observed that some pre-training strategies can only bring marginal improvement, while some even induce negative transfer. Meanwhile, several studies [40, 9, 45] have demonstrated that existing pre-trained molecular representations struggle with challenging yet ubiquitous situations like activity cliffs in drug discovery.

This work aims to enhance molecular representation learning while bridging the gap between domain-agnostic SSL methods and domain-specific molecular tasks. We start by identifying the two major drawbacks in existing methods: Firstly, in contrastive learning, the conventional formulations of the semantic-similar/dissimilar (i.e., positive/negative) samples are not well-tailored for molecular graphs. Most graph contrastive methods generate positive samples via graph perturbation, such as atom masking, bond deletion/addition [50, 21, 42, 47], and subgraph masking [42] in terms of the molecular graphs. However, chemical validity might be challenged by the perturbation (e.g., randomly breaking a bond). Molecules may also lose essential characteristics by perturbing important motifs like aromatic rings, shifting the semantics distant away. The negative samples, taken from the rest of the data, are often treated equally. It essentially neglects the existing molecule structural relationship and the presence of specific molecular components; Second, almost all existing works attempt to learn a *context-independent* molecular representation space, aiming to generalize to various applications. However, this contradicts the fact that molecular properties are often *context-dependent*, from both the physical (e.g., surrounding environments) and biological (e.g., interaction with proteins) perspectives. In other words, it remains uncertain whether the same SSL tasks learned in pre-training could align well with diverse tasks of distinct properties in fine-tuning, thereby leading to the learning gap.

To approach the aforementioned challenges, we introduce a prompt-guided multi-channel learning framework for molecular representation learning using graph neural networks (GNNs). Each of the k channels, guided by a specific prompt token, is responsible for learning one dedicated SSL task. Essentially, the pre-trained model is able to learn k distinct representation spaces. During fine-tuning, a prompt selection module is optimized to aggregate k representations into a composite representation, which is used for molecular property predictions. This involves determining which prompt-guided information channel is most relevant to the current application, thereby making the representation *context-dependent*. The prompt selection module is initialized by identifying the composite representation with the smoothest quantitative structure-property landscape [2]. We later show how this composite formulation is more resilient to label overfitting and manifests better robustness. We design the SSL tasks to form an interpolation from a global view to a local view of the molecular structures. Besides leveraging the *global* molecule contrastive learning [42] and the *local* context prediction [30], we introduce a novel task called the scaffold contrastive distancing, highlighting the foundational role of scaffolds in affecting molecular characteristics and behaviors. Inspired by the facts that scaffolds are often treated as starting points for new compound design, scaffold distancing aims to map

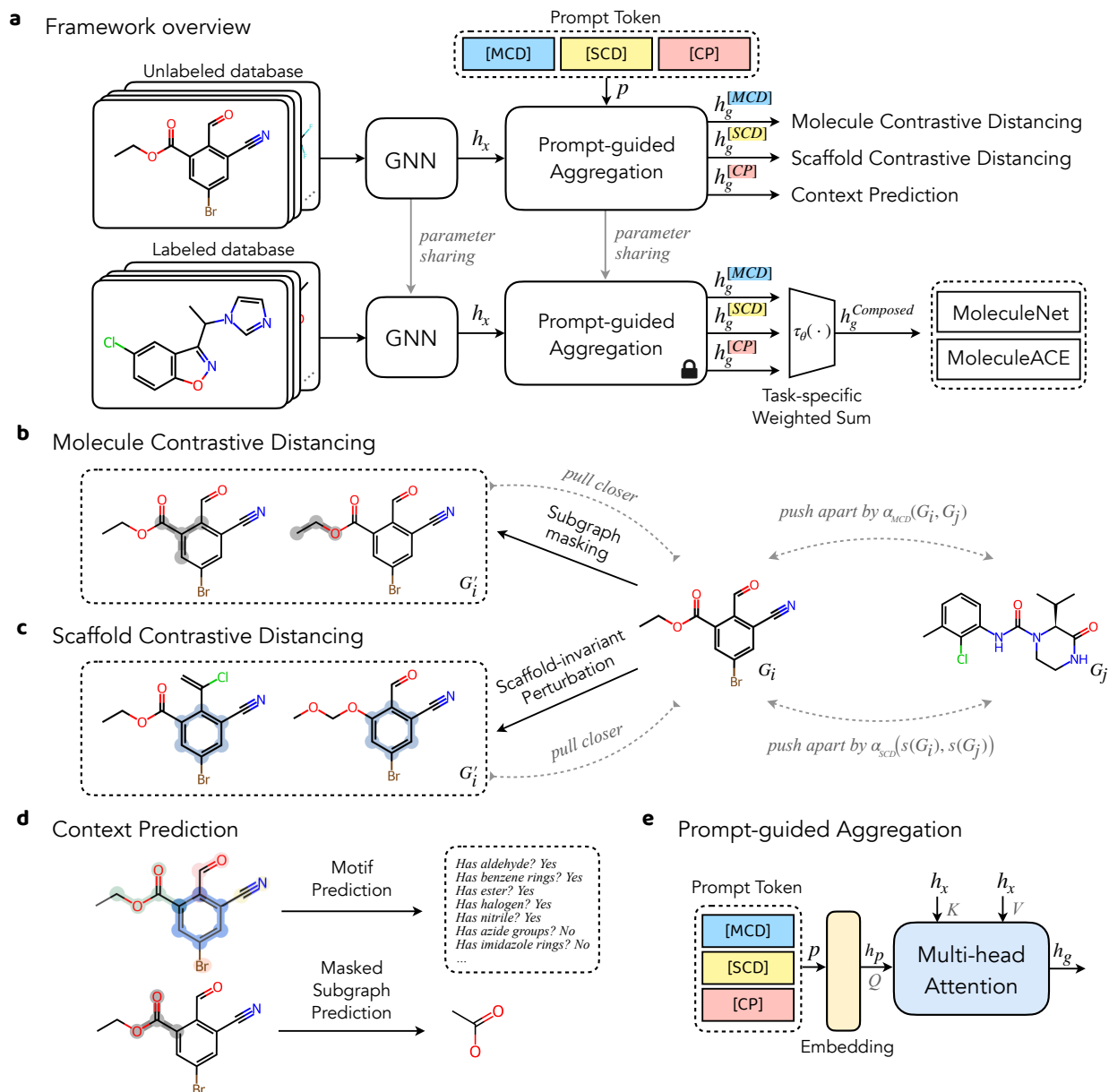


Figure 1: **Framework overview.** **a)** The prompt guided pretrain-finetune framework. For each downstream task, the model is optimized additionally on the prompt weight selection, locating the best pre-trained channel compatible with the current application. **b)** Molecule contrastive learning, where the positive samples G'_i from subgraph masking is contrasted against negative samples G_j by an adaptive margin. **c)** Scaffold contrastive distancing, where the positive samples G'_i from scaffold-invariant perturbation is contrasted by against negative samples G_j by an adaptive margin. **d)** Context prediction channel consists of masked subgraph prediction and motif prediction tasks. **e)** Prompt-guided aggregation module, which conditionally aggregates atom representations into molecule representation by prompt token. It is realized via a multi-head attention with prompt embedding h_p being the query.

molecules with similar scaffolds (generated via *scaffold-invariant perturbations*) closer in the representation space. Additionally, it pushes molecules with different scaffolds apart, where the distance margin is computed adaptively based on scaffold composition difference. Note that the scaffold distancing tackles the partial but core view of the molecules. The overall framework is pre-trained using ZINC15 [33], and evaluated

on 7 molecular property prediction tasks in MoleculeNet [46] and 30 binding potency prediction tasks in MoleculeACE [40]. Learning to leverage information from different channels for different applications, our method surpasses various baseline representation learning methods in both benchmarks. Moreover, our method is shown to handle the challenge of activity cliffs more effectively, whereas competing approaches are more susceptible to the negative transfer, leading to substantial performance decline. Besides reporting the performance metrics, we further examine the shift in representation space during fine-tuning via epoch probing, and discover that our learned representation is better at preserving pre-trained chemical knowledge with better transferability and robustness compared to other baselines. Case study shows that our method has the potential to identify crucial patterns that contribute to activity cliffs even using merely topological cues. We also demonstrate that the learned channel-wise representation distances are highly correlated with the conventional fingerprint/descriptor similarity. These representations can form an implicit representation hierarchy, visualized by iteratively refining the chemical space clustering.

2 Results

2.1 Framework overview

The proposed framework (Figure 1) comprises three novel components compared to the conventional pretrain-finetune paradigm on molecules: (1) The prompt-guided multi-channel learning, (2) contrastive learning with adaptive margin, and (3) scaffold-invariant molecule perturbation.

Prompt-guided multi-channel learning We introduce a prompt-guided multi-channel learning framework for molecular representation learning using GNNs, as shown in Figure 1a. Essentially, the molecular graphs will first go through a unified GNN module, and then diverge into k different channels, each of which is responsible for learning distinct SSL tasks. For each channel, a prompt token p_i is utilized to guide the molecule representation. This is realized via a prompt-guided readout operation [23], which aggregates atom representations conditionally into molecule representation given the prompt token (Figure 1e). Our experiment involves three learning channels, which are molecule distancing, scaffold distancing, and context prediction. Each channel focuses on a unique aspect of the molecular structure, enabling molecular representation learning from an hierarchical viewpoints, from a global view (i.e., entire molecule), a partial view (i.e., core structure), and down to a local view (i.e., functional groups).

We now briefly introduce the three learning channels. (i) Molecule distancing (Figure 1b) is similar to MolCLR [42], where subgraph masking is adopted for molecule augmentation, and the augmented molecules are contrasted against other molecules. We formulate our contrastive learning using the triplet loss [31]. It considers triplet of data samples {anchor, positive, negative}, where negative (i.e., dissimilar) samples are pushed apart against anchor and positive (i.e., similar) samples by a margin α . On top of this, we propose the *adaptive margin loss*, as detailed below. It introduces another level of distancing constraints based on the structural similarity of molecule composition. (ii) We propose scaffold distancing (Figure 1c) as a novel contrastive learning task that focuses on scaffold differences. Molecule scaffolds are often viewed as the foundation for a range of biologically active molecules. They play a crucial role in drug discovery and medicinal chemistry by providing a starting point for the design of new compounds with desired pharmacological properties. In other words, molecules with similar scaffolds are more likely to possess similar physical (e.g., solubility, lipophilicity) and biological (e.g., conformational property when interacting with a protein) characteristics, and thereby sharing similar semantics. Scaffold distancing contrasts the *scaffold-invariant molecule perturbations*, as detailed below, against the other molecules with different scaffolds using the *adaptive margin loss*. (iii) Context prediction (Figure 1d) involves masked subgraph prediction and motif prediction, which are also adopted in GROVER [30]. For each molecular graph, a random subgraph (i.e., a center atom and its one-hop neighbors) is masked out, and the model aims to predict this masked portion based on its surrounding structures. Motif prediction aims to predict the existence of functional groups in the molecule. Both of them are formulated as multi-label classification tasks. Note that this learning channel mainly focuses on the local view of the molecule by identifying the existence of substructure and functional groups, while molecule distancing and scaffold distancing focus more on the global view and partial view, respectively.

In the fine-tuning stage, the model consists of the same GNN and prompt-guided aggregation modules, whose parameters are initialized from the pre-trained model. The parameters in the aggregation modules are fixed during finetuning as we aim to use it as a pooling layer independent of the downstream applications. In addition, a prompt-tuning module $\tau_\theta(\cdot)$ is introduced in fine-tuning to determine which channel is most relevant to the current application. It essentially learns a task-specific prompt distribution. The prompt weights are utilized to linearly combine the channel-wise information into a composite molecule representation, which is then used for the task-specific prediction. We initialize the prompt prompts by choosing the candidate which leads to the smoothest quantitative structure-property landscape (i.e., lowest roughness index) [2] of the composite representation. The framework is then evaluated on both the molecular property prediction and binding potency prediction benchmarks. More details are included in the Method section.

Contrastive learning with adaptive margin We further introduce the adaptive margin loss, a variant of the triplet contrastive learning loss [31], that supports the contrastive learning in the first two channels (molecule distancing and scaffold distancing). In the conventional triplet loss, the representation distance between the anchor G_i and negative (i.e., semantic-dissimilar) sample G_j needs to be at least by margin α larger than the distance between the anchor G_i and positive (i.e., semantic similar) sample G'_i . Conventional contrastive learning methods use the same margin for any triplet considered. However, when applied to molecule triplets, it neglects the known structural relationship between molecules (e.g., co-existence of functional groups). To learn a more fine-grained molecule representation space, we propose to dynamically compute the molecule triplet margin based on the Tanimoto similarity between structural fingerprints. As shown in Figure 1b and c, the adaptive margin $\alpha_{\text{MCD}}(\cdot)$ considers the molecule structural similarity between G_i and G_j , while $\alpha_{\text{SCD}}(\cdot)$ considers the scaffold structural similarity between $s(G_i)$ and $s(G_j)$. Another issue with the conventional triplet loss is that it imposes no constraint on the representation space beyond the margin. It means that the actual representation distances are not necessarily to be well correlated with the computed margin, even if the margin constraints are fully satisfied. This is further elaborated by an example in Supplementary Information. Therefore, we include a secondary term into the adaptive margin loss by considering the structural relationship among the anchor and different negative samples. Detailed formulation of the adaptive margin loss is included in Method section. With careful consideration of existing structural similarity, the learned representation space would better capture molecule relationships in a fine-grained representation space.

Scaffold-invariant molecule perturbation To generate semantic-similar samples (i.e., positive) for scaffold contrastive distancing, we propose to perturb only the terminal side chains of the molecule. In other words, the molecule scaffold (i.e., core structure) is preserved. This is done by first identifying the side chains and then performing fragment replacement based on a candidate fragment pool. To avoid significant alterations in molecule characteristics, we restrict the amount of changes to be fewer than five atoms. For simplicity reason, we consider the Bemis-Murcko framework as the scaffold. Figure 1c shows a sample perturbation with scaffolds highlighted in blue. In this example, the benzene ring is the identified scaffold, and either the carboxylic ester group or the carbonyl group is perturbed by another functional groups. Note that such perturbation is not limited to atom-level or bond-level editing, but also motif-level.

2.2 Molecular property prediction

To demonstrate the effectiveness of our approach, we first evaluate it on seven challenging classification tasks from MoleculeNet [46], which is a large-scale curated benchmark that covers multiple molecular property domains (e.g., physiology, biophysics). The scaffold split scheme [19] is applied. The performance is evaluated by the ROC-AUC value. Each experimental result is averaged over three different runs following the prior works [42, 30, 12]. We compare our method with seven competitive molecular representation learning baselines, which cover a wide variety of pre-train SSL techniques and also include the state-of-the-art on the same benchmark dataset. Specifically, we first consider four contrastive SSL baselines: 1. GraphLoG [50] achieves a hierarchical prototypical embedding space with the conventional graph perturbation techniques; 2. D-SLA [21] proposes the discrepancy learning to refine the embedding space with the conventional graph perturbation techniques; 3. MolCLR [42] adapts the NT-Xent [6] contrastive loss with molecule perturbation techniques, including atom/bond editing and subgraph removal; 4. KANO [13] introduces the knowledge

graph prompting techniques to augment molecular graph, while the augmentations are also learned in the contrastive manner. Besides, we include three predictive SSL baselines: 5. Hu et. al [18] adopts masked attribute prediction and molecule subgraph prediction; 6. GROVER [30] proposes a graph Transformer architecture and applies context prediction learning; 7. GEM [12] utilizes the geometric information of molecules and perform bond angle and atom distance prediction. We also include the setting of training GNN from scratch (i.e., No-Pretrain). Table 1 shows the performance comparison results. Our approach improves over the *No Pre-train* setting by 12.4% ROC-AUC in average. When compared to the other SSL methods, our approach reaches the new state-of-the-art performance on BBBP, Clintox, and BACE datasets, while remaining highly competitive in the rest of the tasks. Our overall ROC-AUC score is 1.8% higher than the second best method (GEM).

2.3 Binding potency prediction

We consider MoleculeACE [40] as the second evaluation benchmark. It consists of 30 datasets retrieved from ChEMBL [14]. Each dataset contains binding potency measures (e.g., K_i value) of molecules against a macromolecular targets. These datasets mainly focus on the structure-property relationships (SPR), where the phenomenon of activity cliffs is amplified. Activity cliffs refer to the cases where small changes in molecular structure significantly alters its biological activity, and understanding them is crucial for optimizing lead compounds and designing new molecules with desired activities. The phenomenon is also counter-intuitive in machine learning, as the machine learning model tends to make similar predictions given similar inputs. Stratified sampling is used in data splitting with the activity cliff label. We take R-squared as the evaluation metrics since relative binding potency ranking is more important than absolute prediction errors (e.g., RMSE) in the real world.

Table 2 shows the performance comparison results. The performance variation of *No Pre-train* indicate that these tasks cover different levels of difficulty, regardless of size of the datasets. Our method outperforms the baselines by a large margin in 24 out of 30 tasks. The largest performance gain occurs at the dataset CHEMBL2034_Ki, where the R-squared value is improved by 35%. Surprisingly, all baseline methods suffer a certain degree of negative transfer. GraphLoG has negative transfer on 25 datasets, MolCLR on 17 datasets, and GROVER on 18 datasets. We argue that one of the reasons MolCLR has less negative transfer than GraphLoG is because its sample perturbation method is relatively more tailored for molecules. The results demonstrate that the generic graph pretraining methods might be inefficient in modeling challenging molecular tasks, which is consistent with the finding in [36]. The convergence rate analysis is included in Supplementary Information.

2.4 Representation robustness

To study the robustness of the learned molecule representation, we propose to probe the fine-tuning process and evaluate the shift in the representation space. Essentially, the shift captures how much the pre-trained chemical knowledge is distorted during fine-tuning. We examine the representation space of both the training and validation molecule set at five training timestamps. To clarify, the term "learned representation" refers to the numerical embedding generated after the atom aggregation, before it is fed to the prediction layer. We choose CHEMBL237_Ki, one of the largest binding potency prediction dataset in MoleculeACE, for the downstream target. We compare our method with GraphLoG and MolCLR, as these models only differ by molecule SSL strategies, while using the same GNN architecture and hyperparameters. In Figure 2, each column represents a training timestamp, and each row pair represents the mapping in training and validation molecule space by a specific method. The coloring represents the normalized potency labels. We also report four additional metrics that capture the representation characteristics along the training process: 1. *Roughness Index* (i.e., ROGI) [2] captures the landscape roughness of molecular property given a representation. Small ROGI value indicates better modellability. 2. *Rand Index* [20] measures the similarity between two clusterings. To study the amount of structural information encoded in the representation, we compute the Rand index between clusters formed using Morgan fingerprint (shown by the grey circle) and clusters formed using the current representation. Higher Rand index means more overlaps between clusters, and subsequently more structural information encoded. The change in Rand index also suggests the degree of representation shift. 3. *Cliff-noncliff Distance Ratio* indicates the generalizability of the representation

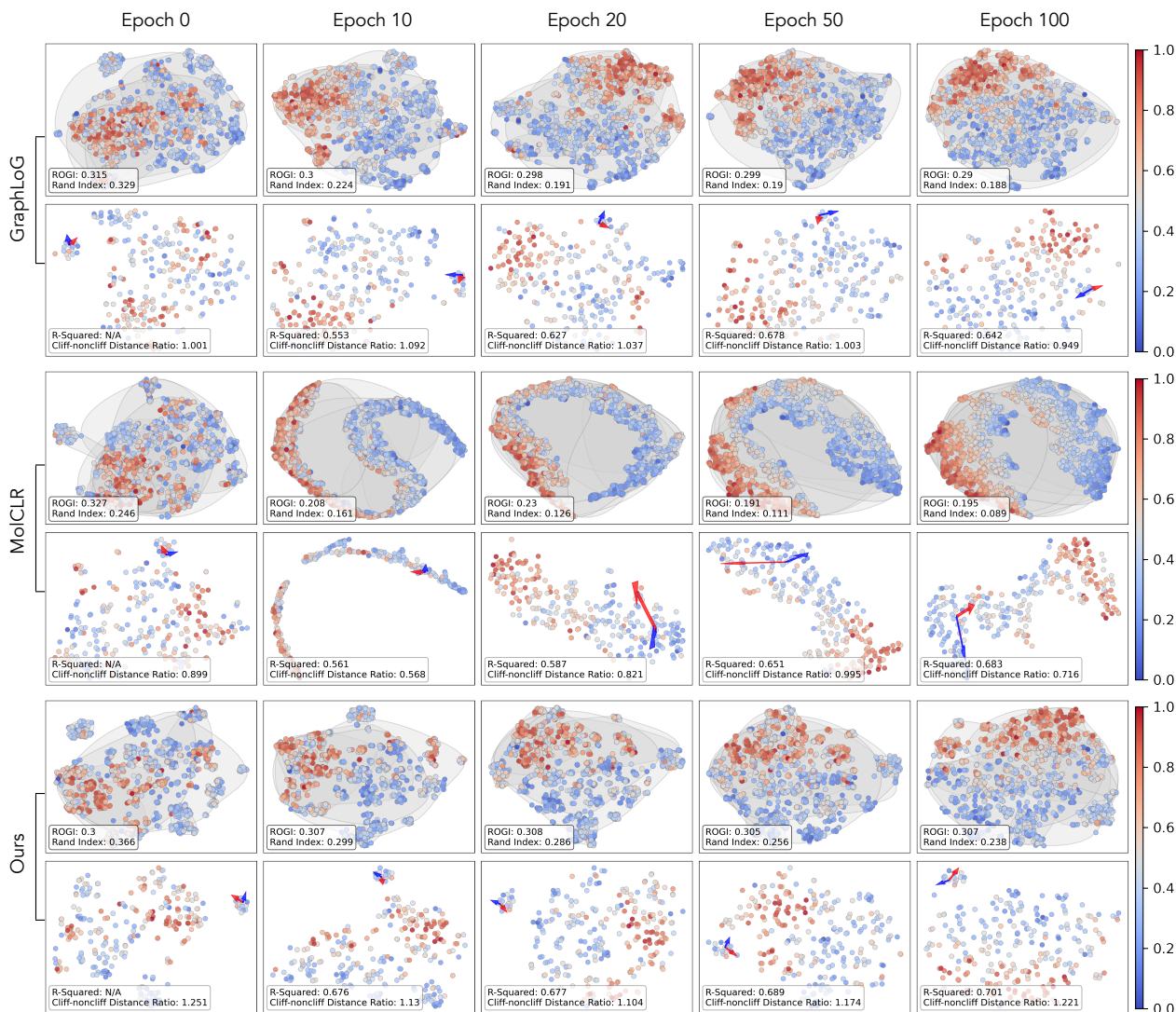


Figure 2: **Representation space probing.** The dynamics of molecule representation space of three methods at five fine-tune timestamps on dataset CHEMBL237_Ki. For each row pair, a 2-D view of the representation space of both the training (top) and validation set (bottom) are visualized. The dot coloring represents the normalized potency labels. Rand index and roughness index are reported for training, while R-squared value and cliff-noncliff distance ratio are reported for validation. The red arrow indicates the distance of a cliff molecule pair, while the blue arrow indicates that of a non-cliff molecule pair.

towards the activity cliff phenomenon. In short, cliff molecule pairs (i.e., similar molecules with different labels) should be more distant away compared to the non-cliff molecule pairs (i.e., similar molecules with similar labels). This is computed on the validation set. We also pin-point three molecules for illustrative purpose, with one cliff pair (indicated by the red arrow) and one non-cliff pair (indicated by the blue arrow). 4. At last, we report the validation *R-squared* for the out-of-sample performance. Here are the three main takeaways from Figure 2:

- With the prompt weight initialization, our composed representation yields the lowest ROGI value to start with. In other words, our pre-trained knowledge can be better transferred to the target application. This is also shown by our rapid convergence rate in the validation set, reaching a validation R-squared of 0.676 at epoch 10.

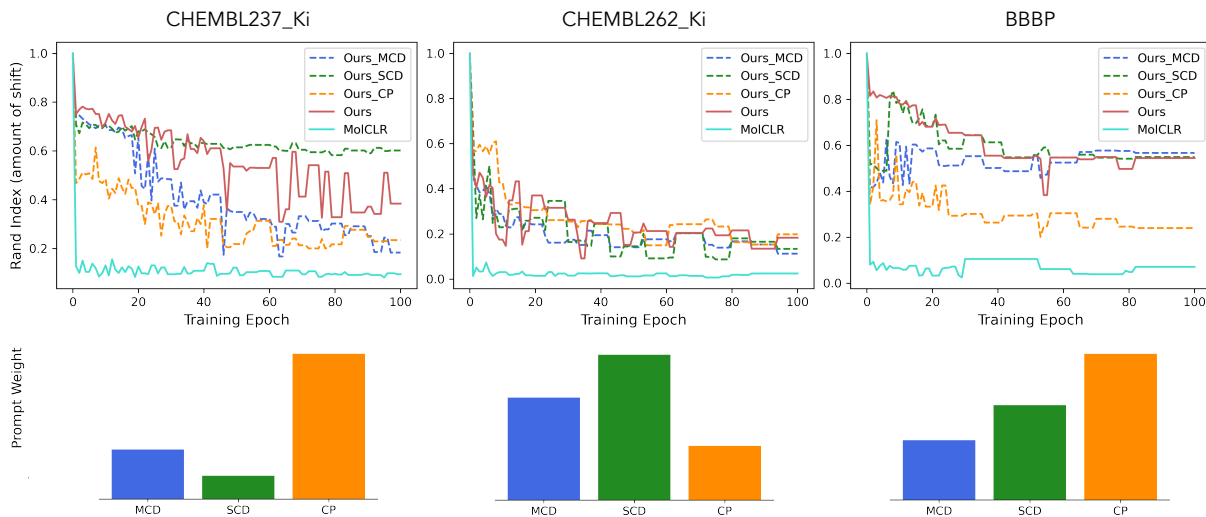


Figure 3: **Representation shift decomposition.** Detailed analysis of the representation shift during fine-tuning across three datasets. The dashed lines (top row) correspond to the representation shift (approximated by the Rand Index) for each individual channel, while the solid lines represent the overall method. The bottom row displays the optimized prompt weights distributed over channels.

- Our representation preserves the structural information better than others, leading to better robustness. While representations are optimized towards the downstream property labels, the Rand index drops continuously for all methods. It means that the encoded information gradually shifts from being structure-oriented to label-oriented. However, our method has the lowest Rand index drop of 0.128, compared to the drop of 0.141 by GraphLoG and 0.157 by MolCLR. The visualization also shows that the representation space of MolCLR gradually becomes label-centric (i.e., overfitting), while losing structural relationship between molecules. This explains its low ROGI value and low validation R-squared along the training process.
- Our representation exhibits a better understanding of the concept of activity cliffs. Our cliff-noncliff distance ratio in the validation set is always positive and larger than that of GraphLoG and MolCLR. As illustrated by the triplet samples, the red arrow is always larger than the blue arrow, while the closeness of cliff and non-cliff pairs in space (i.e., structurally similar) is being maintained. For MolCLR, even though the red arrow is much longer than the blue one at some timestamps, the triplet points are distant away from each other. It means that MolCLR fails to capture the structural similarity aspect of the activity cliffs.

To further understand why our composed representation is more resilient to the representation shift and can better preserve pre-trained knowledge, we present more analysis on three diverse datasets, along with the individual channel-wise representation behavior during fine-tuning. We choose CHEMBL237_Ki and CHEMBL262_Ki as the representative regression-based datasets of different scales, and BBBP as the typical classification-based dataset. The Rand index of representation clustering difference between the initial and the current timestamp is computed as a proxy for the representation shift. A smaller Rand index indicates a larger shift. As illustrated in Figure 3, channels with the highest prompt weights often exhibit the largest shift, and vice versa. This is reasonable because these channels contribute more to the optimization against the labels. Conversely, even though low-weighted channels contribute less to the optimization, they are more likely to preserve the pre-trained knowledge. As a result, the composed representation derived from channel aggregation exhibits a certain level of resilience to representation shifts, making it potentially more robust than other methods. We also include a few-shot representation probing analysis in Supplementary Information, which demonstrates similar patterns.

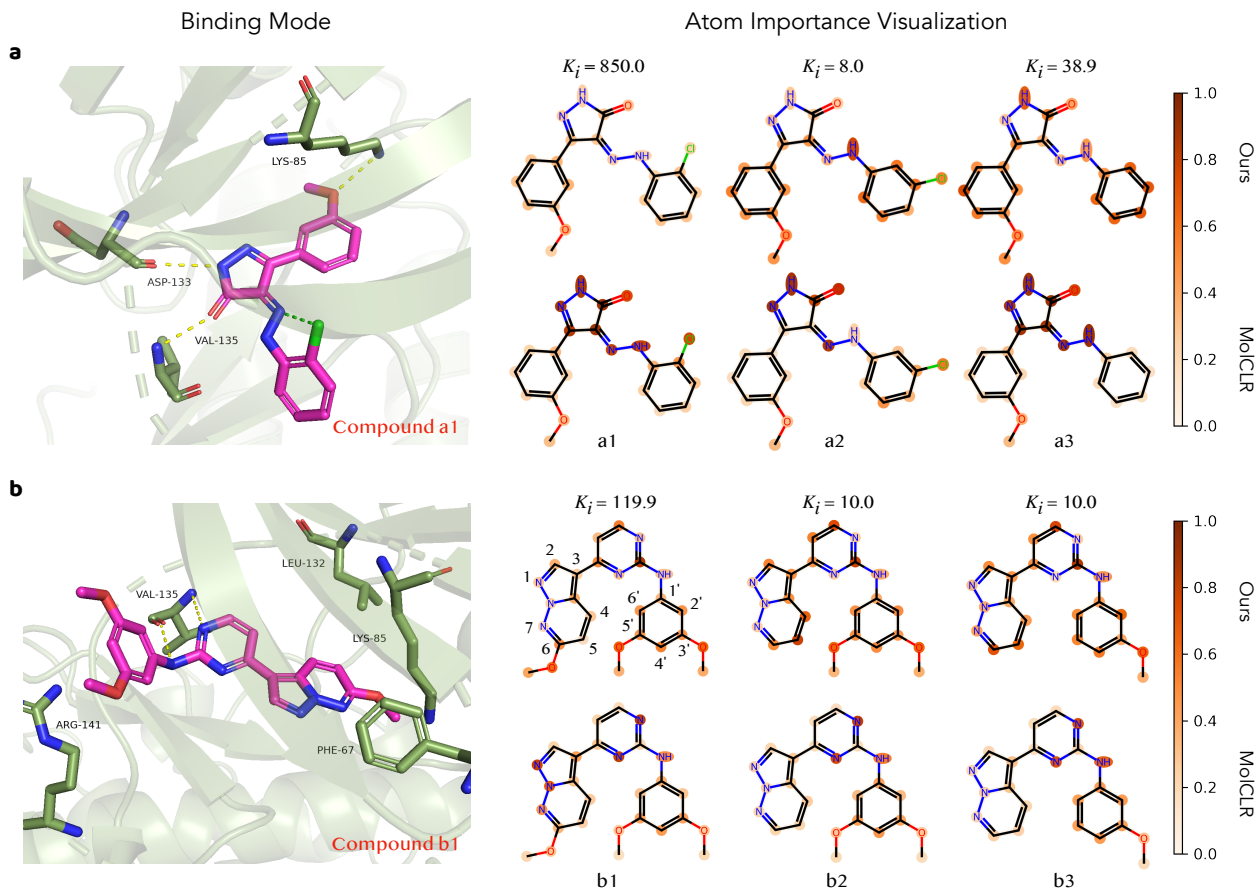


Figure 4: **Activity cliffs analysis.** Evaluate the bioactivity binding mode and the atom importance captured by our model on a (a) 5-phenyl-4-phenyldiazenyl-1,2-dihydropyrazol-3-one series and a (b) N-phenyl-4-pyrazolo[1,5-b]pyridazin-3-ylpyrimidin-2-amine series. The binding modes of compound *a1* and compound *b1* in the active sites of GSK3 β (PDB ID: 3L1S) are predicted by AutoDock Vina and visualized by PyMOL [7]. The key hydrogen bonds between compounds and the active sites are highlighted by yellow dash lines, while the green dash line refers to the intra-molecular halogen bond. The color intensity on each atom indicates its respective contribution to the prediction of our method, computed from a GNNExplainer.

2.5 Activity cliffs analysis

We present a deeper analysis into the potential of our method in understanding the activity cliffs. To be more specific, we evaluate the relationship between the model explanations generated by the GNNExplainer [51] and the predicted binding mode between the ligands and the protein pockets by AutoDock Vina [38]. Note that this analysis merely serves as a proof of concept, such that our representation has the potential of capturing influential and well-established factors in binding affinities. However, the fundamental limitation of utilizing topological information only is unavoidable, which we will discuss in Conclusion.

As shown in Figure 4, two series of compounds sharing the same scaffolds are potential inhibitors of glycogen synthase kinase-3 beta (GSK3 β). The molecule activity cliff pairs, determined by the formulation in [40], are compounds $\langle a1, a2 \rangle$, $\langle a1, a3 \rangle$, $\langle b1, b2 \rangle$, and $\langle b1, b3 \rangle$. The explanations of both our and MolCLR’s predictions are compared. In Figure 4a, the potential intra-molecular halogen-bonding contact between the chlorine atom and hydrazone in compound *a1*, as indicated by the green dashed line, is disfavored for the inter-molecular hydrogen-bonding contact between the backbone carbonyl of the active site VAL-135 and hydrazone of the compound [3]. As shown by our model explanation, compared to the compound *a2* and *a3*, the chlorine atom of compound *a1*, along with its associated benzene ring, contribute less to the overall binding affinity prediction. It aligns well with the predicted binding mode.

The predicted binding mode in Figure 4b shows that the orientation of the substituent (i.e., the alkoxy group in compound *b1* at the 6 position of pyrazolo[1,5-b]pyridazine) will cause steric clash with PHE-67 in the G-rich loop of GSK3 β , thereby leading to a loss of potency [37, 34]. In contrast, the alkoxy groups at the 3' and 5' positions have no clear contact with the protein pocket. Remarkably, using only the topological information, our model can capture the importance of the influential alkoxy group at 6 position. In addition, the absence of the alkoxy group at 5' position (from compound *b2* to *b3*) does not affect the overall atoms' contribution to the predicted potency. MolCLR performs equally good in terms of compound *b2* and *b3*, but it fails to capture the influential alkoxy group in compound *b1*.

3 Discussion

In this work, we propose a novel multi-channel learning framework for molecule representation learning. Each channel is dedicated to learning one self-supervised learning task, with varying levels of focus on the global and local aspects of the molecule. Specifically, the molecule contrastive distancing captures the molecule's global similarity, the scaffold contrastive distancing highlights the foundational role of the scaffold in affecting molecular characteristics, and the context prediction targets the composition of functional groups. Further analysis shows that representations learned from these channels form an implicit feature hierarchy. When fine-tuned on downstream tasks, the model is able to identify which channel-wise representation is most relevant to the current application, thereby making the composite representation *context-dependent*. It mitigates the learning gap between pre-training and fine-tuning objectives. In addition, the composite formulation endows our representation with enhanced robustness and generalizability, shown by its resilience to representation shifts and label overfitting.

There are several interesting directions for future research. One of the potential improvements is to consider more the interaction between channels. Currently, the GNN's message-passing module is shared across channels, whereas there is no explicit guidance on inter-channel correlations. For instance, is it possible to explicitly formulate a representation hierarchy during pre-training? Another promising direction is to incorporate 3D geometric information into the framework. By merely leveraging topological molecular structure, the model is unable to differentiate molecules with different conformations (e.g., functional groups' orientation or atom's chirality), which are fundamental in bioactivity prediction. Besides, there exist other advanced data-driven techniques for studying the structural-activity relationship (SAR) that might be compatible with our framework. For example, Molecular Anatomy [24] argues that the network clustering from scaffold fragmentation and abstraction allows high quality structure-activity relationships (SAR) analysis. Such investigations aim to transfer knowledge from cheminformatics to machine learning models, potentially improving both model interpretability and robustness. More importantly, while our method has immediate implications for drug discovery, its molecular representation robustness further shed lights on its promising potential in other sub-fields of chemistry, such as materials science and environmental chemistry.

4 Methods

Graph neural networks (GNNs) A graph $G = (V, E)$ is defined by a set of nodes V and edges E . In the molecular graph, each node denotes an atom, and the edge denotes the chemical bond. Let h_v be the representation of node v , and h_G be the representation of the graph G . Modern GNNs follow the message-passing framework, such that node representations are updated iteratively via neighborhood aggregation:

$$h_v^k = \text{UPDATE}(h_v^{k-1}, \text{AGGREGATE}(\{h_v^{k-1}, h_u^{k-1}, e_{uv}\} : \forall u \in N(v))) ,$$

where $N(v)$ is the neighborhood of node v , k denotes the layer index in a multi-layer GNN structure, and e_{uv} denotes the edge connecting two nodes u and v . The initialization of h_v^0 comes from the predefined node features x_v . The aggregate function integrates neighborhood information into the current node representation. The update function takes the updated node representation and the node representation from the previous $k - 1$ layer and performs operations like concatenation or summation. After the iterative updates, a permutation-invariant pooling operation is performed to get the representation for the entire graph G :

$h_g = \text{READOUT}(h_v^k | v \in V)$. There are various number of options for the readout operation, including simple operations of mean and max, and advanced differentiable approaches like DiffPool [52] and GMT [4].

Prompt-guided aggregation Instead of using the readout operations mentioned above, we adopt the prompt-guided aggregation, which is achieved using the multi-head attention. As shown in Figure 1e, the embedding of the prompt token h_p is treated as the attention query, while the representations h_x of nodes/atoms x , are viewed as the keys and values. The resulted prompt-aware graph representation $h_g^p = \sum_x \alpha_x h_x$, where the attention weight for each node x is computed as $\alpha_x = \text{softmax}(\{q \cdot k_x / \sqrt{d_k}\}_x)$, and $q = W_q h_p$, $k_x = W_k h_x$, and $v_x = W_v h_x$. Here $\{W_q, W_k, W_v\}$ represent parameters in the linear transformations, and $\sqrt{d_k}$ is the scaling factor. Essentially, the prompt-aware h_g^p is aggregated from the weighted average of h_x .

Adaptive margin contrastive loss Contrastive learning is a technique widely used in self-supervised learning, which aims to group semantic similar samples closer while pushing dissimilar samples distant apart in the latent representation space. In this work, we adopt the triplet loss [31] to formulate the contrastive learning. It considers triplets of data samples: the anchor G_i , the positive (i.e., semantic-similar) sample G'_i , and the negative (i.e., semantic-dissimilar) sample G_j . Its formulation is shown below.

$$\ell_{i,j(\neq i)} = \max(0, \alpha + d(\mathbf{h}_{g_i}, \mathbf{h}'_{g_i}) - d(\mathbf{h}_{g_i}, \mathbf{h}_{g_j})) , \quad (1)$$

where \mathbf{h}_{g_i} denotes the latent representation for sample G_i , and \mathbf{h}'_{g_i} being the representation for its augmentation. The function $d(\cdot, \cdot)$ measures the L2 distance between two vectors. In general, this objective enforces the pair-wise distancing difference between $\langle G_i, G'_i \rangle$ and $\langle G_i, G_j \rangle$ to be at least α margin. However, as we discuss before, this formulation can only lead to a coarse-grained representation space, while neglecting the existing structural relationship among molecules (e.g., shared rings or functional groups). Also, this formulation does not pose any constraints on the representation space beyond the margin (see Supplementary Information for example illustration). Therefore, we propose to add an additional contrastive formulation with adaptive margin among negative samples and the anchor.

$$\begin{aligned} \ell_{i,j(\neq i),k(\neq j \neq i)} = & \max(0, \alpha_1(G_i, G_j) + d(\mathbf{h}_{g_i}, \mathbf{h}'_{g_i}) - d(\mathbf{h}_{g_i}, \mathbf{h}_{g_j})) + \\ & \max(0, \alpha_1(G_i, G_k) + d(\mathbf{h}_{g_i}, \mathbf{h}'_{g_i}) - d(\mathbf{h}_{g_i}, \mathbf{h}_{g_k})) + \\ & \max(0, \alpha_2(G_i, G_j, G_k) + d(\mathbf{h}_{g_i}, \mathbf{h}_{g_j}) - d(\mathbf{h}_{g_i}, \mathbf{h}_{g_k})) , \end{aligned} \quad (2)$$

where $\alpha_1(\cdot)$ and $\alpha_2(\cdot)$ are the adaptive margin functions. Let \mathbf{z}_{g_i} be the conventional structural features of the sample G_i . We use the Morgan fingerprint [25], which hashes circular atom neighborhoods into fixed-length binary strings, to represent the structural features. In molecule contrastive distancing, the adaptive function $\alpha_1(G_i, G_j) = \alpha_{\text{offset}} \times (1 - \text{sim}(\mathbf{z}_{g_i}, \mathbf{z}_{g_j}))$, and $\alpha_2(G_i, G_j, G_k) = \alpha_{\text{offset}} \times (\text{sim}(\mathbf{z}_{g_i}, \mathbf{z}_{g_j}) - \text{sim}(\mathbf{z}_{g_i}, \mathbf{z}_{g_k}))$, where $\text{sim}(\cdot, \cdot)$ denotes the Tanimoto similarity. The scaffold contrastive distancing has the same formulation, except that the molecule sample G is replaced by its scaffold $s(G)$. Note that the formulation now considers quadruplet of data samples $\langle G_i, G'_i, G_{j(\neq i)}, G_{k(\neq j \neq i)} \rangle$. Even though the theoretical complexity is increased from $O(N^2K)$ to $O(N^3)$, we can perform fixed-size random sampling with respect to the computed similarity differences in $\alpha_2(\cdot)$. Quadruplets are also dropped if the computed values are negative. Eventually, the optimization goal is to minimize the loss summation as $\min \sum_{i,j,k} \ell_{i,j(\neq i),k(\neq j \neq i)}$.

Prompt-guided multi-channel learning The overall multi-channel learning framework is inspired by the work in [43]. At the pre-train stage, each channel is responsible for learning distinct SSL tasks that focus on a unique aspect of the molecule. At the fine-tune stage, the model parameters learned via pre-training are first used to initialize the fine-tune model. Besides, we introduce an additional prompt selection module to combine representations from different channels into the task-specific (i.e., context-dependent) composite representation. Essentially, it learns the relevance between different pre-trained molecular knowledge and the downstream application, hence bridging the gap between pre-training and fine-tuning objectives. Through experiments, we find that directly optimizing the pre-trained multi-channel model with randomly initialized prompt weights could easily reach local optimum. In other words, the downstream performance is sensitive to the random initialization of selected prompts. Therefore, we propose a prompt weight initialization

trick, such that the initial prompt weights should lead to a composite representation with the smoothest quantitative structure-property landscape (i.e., low ROGI value) [2] with respect to the current application. ROGI measures the roughness of the molecule property landscape given a molecular numeric representation. A low ROGI value indicates better modellability. We use a simple Bayesian optimization pipeline to find the best initialization with the lowest ROGI value on the training set. Essentially, the input parameters of the Bayesian optimization are $k - 1$ learnable scalars, where k is the number of channels. The black-box utility function first computes the distribution over k values by treating the input scalars as logits, and calculates the composite representation as well as its corresponding roughness index. We utilize the Quasi MC-based batch Expected Improvement as the acquisition function. After the initialization, the entire model, except for the prompt-guided aggregation modules, is optimized towards the molecular property labels. The parameters within the prompt-guided aggregation modules are fixed because these layers are set to perform application-agnostic pooling operations over the molecular graph. Hypothetically, the aggregation module responsible for scaffold contrastive distancing should allocate greater attention weight on atoms constituting the scaffold.

Experimental setup We pre-train our framework using the molecules from ZINC15 [33], which is an open-sourced database that contains 2 million unlabelled drug-like compounds. We use CReM [27], an open-sourced molecule mutation framework, for the scaffold-invariant molecule perturbation. To be more specific, we first use RDKit [1] to identify the Bemis-Murcko scaffold of molecules, as well as the connection sites (i.e., atom indices) between the scaffold and the side chains. The CReM algorithm then takes these indices and performs fragment replacement using an external fragment pool. Perturbation results are further filtered by chemical validity and the maximum number of changed atoms allowed. At last, we are able to successfully compute perturbations for 1,882,537 out of 2 million molecules. These molecules form our final pre-train database. In the contrastive-based pre-training, we consider five positive samples for each anchor molecule. In molecule distancing, we randomly apply subgraph masking five times on the original molecule. In scaffold distancing, we randomly sample five scaffold-invariant perturbations. In terms of the model architecture, we follow the same architecture setup as the graph neural network in [50, 18, 42, 21]. We use a 5-layer Graph Isomorphism Network (GIN) [49] as the backbone, whose hidden dimension size is set to 300. For the MoleculeNet benchmark, we utilize the same molecule feature sets as works in [30, 13], while we consider the same molecule feature sets as works in [18, 21, 42, 50] for the MoleculeACE benchmark.

Baselines We replicate the performance of MolCLR, GROVER, GEM, and KANO on the MoleculeNet benchmark using their provided checkpoints and code repositories. Note that the published reported results of GROVER and KANO are evaluated under the balanced scaffold split, which is different than the deterministic scaffold split used in this work and the rest of the baseline methods. For the MoleculeACE benchmark, we again fine-tune GraphLoG, MolCLR, and GROVER using their repositories and model checkpoints.

Representation space probing We propose to analyze the dynamics of representation space during fine-tuning to evaluate the representation robustness and generalizability. To be more specific, we probe the mapping of the representation space at five different training timestamps (epoch 0, epoch 10, epoch 20, epoch 50, epoch 100). The 2-D view is constructed via the T-SNE [39] dimension reduction technique. Besides the visualization, we also report four additional metrics that capture the representation characteristics. We report the ROGI value and Rand index in the training set, plus the R-squared value and cliff-noncliff distance ratio in the validation set. The Rand index is calculated from two clustering assignments. The first clustering is formed using KMeans clustering with the molecule Morgan fingerprint (radius=2, nBits=512). The second clustering is formed with using KMeans clustering with the representation at the current timestamp. We set the same number of clusters for these two clusterings. In terms of the cliff-noncliff distance ratio, we first identify the cliff and the noncliff molecule pairs using the same principle in MoleculeACE [40]. Then, we compute and average the representation distance of each pair. At last, the cliff-noncliff ratio is formed by normalizing their average distance.

Table 1: Fine-tuning results (ROC-AUC) on 7 classification tasks in MoleculeNet. The results of MolCLR, GROVER, GEM, and KANO are taken from rerunning their code repositories using the exact scaffold split.

Methods	BBBP	Clintox	MUV	HIV	BACE	Tox21	SIDER	Avg.
No Pre-train	65.8 \pm 4.5	58.0 \pm 4.4	71.8 \pm 2.5	75.3 \pm 1.9	70.1 \pm 5.4	74.0 \pm 0.8	57.3 \pm 1.6	67.5
Hu et. al [18]	70.8 \pm 1.5	72.6 \pm 1.5	81.3 \pm 2.1	79.9 \pm 0.7	84.5 \pm 0.7	78.7 \pm 0.4	62.7 \pm 0.8	75.8
GraphLoG [50]	72.3 \pm 0.9	74.7 \pm 2.2	74.2 \pm 1.8	75.4 \pm 0.6	82.2 \pm 0.9	75.1 \pm 0.7	61.2 \pm 1.1	73.6
D-SLA [21]	72.6 \pm 0.8	80.2 \pm 1.5	76.6 \pm 0.9	78.6 \pm 0.4	83.8 \pm 1.0	76.8 \pm 0.5	60.2 \pm 1.1	75.5
MolCLR [42]	73.5 \pm 0.4	90.4 \pm 1.7	75.5 \pm 1.8	77.6 \pm 3.2	83.5 \pm 1.8	76.7 \pm 2.1	60.7 \pm 5.7	76.8
GROVER [30]	69.5 \pm 0.1	76.2 \pm 3.7	67.3 \pm 1.8	68.2 \pm 1.1	81.0 \pm 1.4	73.5 \pm 0.1	65.4 \pm 0.1	71.6
GEM [12]	71.8 \pm 0.6	89.7 \pm 2.0	77.0 \pm 1.5	78.0 \pm 1.4	84.9 \pm 1.1	78.2 \pm 0.3	67.2 \pm 0.6	78.1
KANO [13]	69.9 \pm 1.9	90.7 \pm 2.2	74.7 \pm 2.0	75.7 \pm 0.3	82.7 \pm 0.9	75.8 \pm 0.5	60.2 \pm 1.4	75.7
Ours	74.1 \pm 0.6	95.7 \pm 1.2	81.2 \pm 0.5	79.8 \pm 0.3	85.0 \pm 1.1	77.5 \pm 0.3	66.7 \pm 0.8	80.1

Table 2: Fine-tuning results (R-Squared) on 30 binding potency prediction tasks in MoleculeACE.

Dataset	Size	SSL methods				
		No Pre-train	GraphLoG	MolCLR	GROVER	Ours
CHEMBL4203_Ki	731	0.09 ± 0.12	0.05 ± 0.02	0.09 ± 0.05	0.16 ± 0.03	0.24 ± 0.05
CHEMBL262_Ki	856	0.20 ± 0.1	0.34 ± 0.04	0.45 ± 0.02	0.40 ± 0.07	0.50 ± 0.04
CHEMBL2034_Ki	750	0.30 ± 0.06	0.56 ± 0.03	0.40 ± 0.1	0.52 ± 0.02	0.65 ± 0.01
CHEMBL218_EC50	1031	0.35 ± 0.06	0.34 ± 0.03	0.37 ± 0.04	0.48 ± 0.07	0.35 ± 0.03
CHEMBL3979_EC50	1125	0.36 ± 0.04	0.29 ± 0.03	0.35 ± 0.07	0.34 ± 0.05	0.39 ± 0.03
CHEMBL2047_EC50	631	0.41 ± 0.08	0.52 ± 0.02	0.44 ± 0.09	0.59 ± 0.02	0.63 ± 0.04
CHEMBL1871_Ki	659	0.42 ± 0.05	0.33 ± 0.03	0.41 ± 0.09	0.42 ± 0.06	0.49 ± 0.04
CHEMBL4616_EC50	682	0.42 ± 0.06	0.49 ± 0.03	0.48 ± 0.06	0.44 ± 0.1	0.52 ± 0.02
CHEMBL219_Ki	1859	0.44 ± 0.04	0.40 ± 0.04	0.37 ± 0.04	0.32 ± 0.05	0.53 ± 0.03
CHEMBL287_Ki	1328	0.46 ± 0.03	0.21 ± 0.04	0.42 ± 0.05	0.39 ± 0.02	0.49 ± 0.02
CHEMBL239_EC50	1721	0.47 ± 0.06	0.41 ± 0.04	0.47 ± 0.07	0.52 ± 0.02	0.54 ± 0.03
CHEMBL235_EC50	2349	0.52 ± 0.02	0.51 ± 0.04	0.48 ± 0.03	0.40 ± 0.1	0.54 ± 0.01
CHEMBL231_Ki	973	0.58 ± 0.02	0.54 ± 0.03	0.57 ± 0.03	0.64 ± 0.02	0.65 ± 0.02
CHEMBL237_EC50	955	0.60 ± 0.05	0.51 ± 0.03	0.53 ± 0.07	0.52 ± 0.11	0.63 ± 0.02
CHEMBL238_Ki	1052	0.62 ± 0.04	0.56 ± 0.02	0.63 ± 0.06	0.62 ± 0.01	0.65 ± 0.02
CHEMBL233_Ki	3142	0.63 ± 0.01	0.59 ± 0.02	0.64 ± 0.02	0.50 ± 0.09	0.67 ± 0.01
CHEMBL214_Ki	3317	0.63 ± 0.01	0.58 ± 0.02	0.60 ± 0.02	0.45 ± 0.09	0.65 ± 0.01
CHEMBL228_Ki	1704	0.63 ± 0.02	0.52 ± 0.03	0.58 ± 0.03	0.46 ± 0.11	0.62 ± 0.01
CHEMBL4005_Ki	960	0.64 ± 0.03	0.57 ± 0.01	0.44 ± 0.06	0.58 ± 0.07	0.63 ± 0.02
CHEMBL4792_Ki	1471	0.65 ± 0.02	0.55 ± 0.03	0.62 ± 0.04	0.55 ± 0.09	0.66 ± 0.02
CHEMBL264_Ki	2862	0.65 ± 0.03	0.60 ± 0.02	0.62 ± 0.03	0.41 ± 0.04	0.61 ± 0.01
CHEMBL237_Ki	2602	0.66 ± 0.01	0.67 ± 0.02	0.67 ± 0.02	0.60 ± 0.06	0.72 ± 0.02
CHEMBL234_Ki	3657	0.66 ± 0.02	0.60 ± 0.01	0.62 ± 0.04	0.49 ± 0.01	0.70 ± 0.01
CHEMBL236_Ki	2598	0.70 ± 0.02	0.65 ± 0.02	0.68 ± 0.02	0.52 ± 0.09	0.71 ± 0.01
CHEMBL1862_Ki	794	0.71 ± 0.03	0.69 ± 0.03	0.76 ± 0.03	0.75 ± 0.01	0.72 ± 0.02
CHEMBL2971_Ki	976	0.72 ± 0.01	0.68 ± 0.02	0.76 ± 0.06	0.78 ± 0.01	0.76 ± 0.03
CHEMBL204_Ki	2754	0.76 ± 0.02	0.71 ± 0.02	0.72 ± 0.02	0.66 ± 0.01	0.76 ± 0.01
CHEMBL2835_Ki	615	0.78 ± 0.03	0.69 ± 0.04	0.75 ± 0.04	0.70 ± 0.03	0.79 ± 0.01
CHEMBL244_Ki	3097	0.80 ± 0.01	0.78 ± 0.01	0.80 ± 0.02	0.63 ± 0.06	0.80 ± 0.02
CHEMBL2147_Ki	1456	0.88 ± 0.01	0.82 ± 0.01	0.87 ± 0.02	0.85 ± 0.01	0.88 ± 0.01
Average		0.558	0.525	0.553	0.523	0.616
#Negative transfer		-	25	17	18	3

References

- [1] Rdkit: Open-source cheminformatics.
- [2] ALDEGHI, M., GRAFF, D. E., FREY, N., MORRONE, J. A., PYZER-KNAPP, E. O., JORDAN, K. E., AND COLEY, C. W. Roughness of Molecular Property Landscapes and Its Impact on Modellability. *Journal of Chemical Information and Modeling* 62, 19 (Oct. 2022), 4660–4671.
- [3] ARNOST, M., PIERCE, A., TER HAAR, E., LAUFFER, D., MADDEN, J., TANNER, K., AND GREEN, J. 3-aryl-4-(arylhyaazono)-1h-pyrazol-5-ones: Highly ligand efficient and potent inhibitors of gsk3 β . *Bioorganic & medicinal chemistry letters* 20, 5 (2010), 1661–1664.
- [4] BAEK, J., KANG, M., AND HWANG, S. J. Accurate learning of graph representations with graph multiset pooling. In *International Conference on Learning Representations* (2021).
- [5] BÖHM, H.-J., FLOHR, A., AND STAHL, M. Scaffold hopping. *Drug Discov Today Technol* 1, 3 (Dec. 2004), 217–224.
- [6] CHEN, T., KORNBLITH, S., NOROUZI, M., AND HINTON, G. E. A simple framework for contrastive learning of visual representations. *CoRR abs/2002.05709* (2020).
- [7] DELANO, W. L., ET AL. Pymol: An open-source molecular graphics tool. *CCP4 Newsl. Protein Crystallogr* 40, 1 (2002), 82–92.
- [8] DENG, J., SOCHER, R., FEI-FEI, L., DONG, W., LI, K., AND LI, L.-J. Imagenet: A large-scale hierarchical image database. In *2009 IEEE Conference on Computer Vision and Pattern Recognition(CVPR)* (06 2009), vol. 00, pp. 248–255.
- [9] DENG, J., YANG, Z., WANG, H., OJIMA, I., SAMARAS, D., AND WANG, F. A systematic study of key elements underlying molecular property prediction. *Nature Communications* 14, 1 (Oct 2023), 6395.
- [10] DEVLIN, J., CHANG, M.-W., LEE, K., AND TOUTANOVA, K. Bert: Pre-training of deep bidirectional transformers for language understanding. *arXiv preprint arXiv:1810.04805* (2018).
- [11] DOWDEN, H., AND MUNRO, J. Trends in clinical success rates and therapeutic focus. *Nat Rev Drug Discov* 18, 7 (July 2019), 495–496.
- [12] FANG, X., LIU, L., LEI, J., HE, D., ZHANG, S., ZHOU, J., WANG, F., WU, H., AND WANG, H. Geometry-enhanced molecular representation learning for property prediction. *Nature Machine Intelligence* 4, 2 (Feb. 2022), 127–134.
- [13] FANG, Y., ZHANG, Q., ZHANG, N., CHEN, Z., ZHUANG, X., SHAO, X., FAN, X., AND CHEN, H. Knowledge graph-enhanced molecular contrastive learning with functional prompt. *Nature Machine Intelligence* (May 2023).
- [14] GAULTON, A., BELLIS, L. J., BENTO, A. P., CHAMBERS, J., DAVIES, M., HERSEY, A., LIGHT, Y., MCGLINCHAY, S., MICHALOVICH, D., AL-LAZIKANI, B., AND OVERINGTON, J. P. ChEMBL: a large-scale bioactivity database for drug discovery. *Nucleic Acids Research* 40, D1 (Jan. 2012), D1100–D1107.
- [15] GENTILE, F., YAACOUB, J. C., GLEAVE, J., FERNANDEZ, M., TON, A.-T., BAN, F., STERN, A., AND CHERKASOV, A. Artificial intelligence-enabled virtual screening of ultra-large chemical libraries with deep docking. *Nature Protocols* 17, 3 (Mar 2022), 672–697.
- [16] GOH, G. B., HODAS, N. O., AND VISHNU, A. Deep learning for computational chemistry, 2017.
- [17] HAY, M., THOMAS, D. W., CRAIGHEAD, J. L., ECONOMIDES, C., AND ROSENTHAL, J. Clinical development success rates for investigational drugs. *Nat Biotechnol* 32, 1 (Jan. 2014), 40–51.
- [18] HU*, W., LIU*, B., GOMES, J., ZITNIK, M., LIANG, P., PANDE, V., AND LESKOVEC, J. Strategies for pre-training graph neural networks. In *International Conference on Learning Representations* (2020).

- [19] HU, W., LIU, B., GOMES, J., ZITNIK, M., LIANG, P., PANDE, V. S., AND LESKOVEC, J. Pre-training graph neural networks. *CoRR abs/1905.12265* (2019).
- [20] HUBERT, L., AND ARABIE, P. Comparing partitions. *Journal of Classification* 2, 1 (Dec 1985), 193–218.
- [21] KIM, D., BAEK, J., AND HWANG, S. J. Graph self-supervised learning with accurate discrepancy learning. *CoRR abs/2202.02989* (2022).
- [22] KIM, D., AND OH, A. How to find your friendly neighborhood: Graph attention design with self-supervision. In *International Conference on Learning Representations* (2021).
- [23] LIU, Z., YU, X., FANG, Y., AND ZHANG, X. GraphPrompt: Unifying Pre-Training and Downstream Tasks for Graph Neural Networks, Feb. 2023. arXiv:2302.08043 [cs].
- [24] MANELFI, C., GEMEI, M., TALARICO, C., CERCHIA, C., FAVA, A., LUNGHINI, F., AND BECCARI, A. R. “Molecular Anatomy”: a new multi-dimensional hierarchical scaffold analysis tool. *Journal of Cheminformatics* 13, 1 (Dec. 2021), 54.
- [25] MORGAN, H. L. The generation of a unique machine description for chemical structures—a technique developed at chemical abstracts service. *Journal of Chemical Documentation* 5, 2 (1965), 107–113.
- [26] PÉREZ-VILLANUEVA, J., MÉNDEZ-LUCIO, O., SORIA-ARTECHE, O., AND MEDINA-FRANCO, J. L. Activity cliffs and activity cliff generators based on chemotype-related activity landscapes. *Mol Divers* 19, 4 (July 2015), 1021–1035.
- [27] POLISHCHUK, P. CReM: chemically reasonable mutations framework for structure generation. *Journal of Cheminformatics* 12, 1 (Apr. 2020), 28.
- [28] RADFORD, A., WU, J., CHILD, R., LUAN, D., AMODEI, D., SUTSKEVER, I., ET AL. Language models are unsupervised multitask learners. *OpenAI blog* 1, 8 (2019), 9.
- [29] RAMSUNDAR, B., EASTMAN, P., WALTERS, P., PANDE, V., LESWING, K., AND WU, Z. *Deep Learning for the Life Sciences*. O’Reilly Media, 2019. <https://www.amazon.com/Deep-Learning-Life-Sciences-Microscopy/dp/1492039837>.
- [30] RONG, Y., BIAN, Y., XU, T., XIE, W., WEI, Y., HUANG, W., AND HUANG, J. Self-Supervised Graph Transformer on Large-Scale Molecular Data.
- [31] SCHROFF, F., KALENICHENKO, D., AND PHILBIN, J. FaceNet: A unified embedding for face recognition and clustering. In *2015 IEEE Conference on Computer Vision and Pattern Recognition (CVPR)* (Boston, MA, USA, June 2015), IEEE, pp. 815–823.
- [32] SHERIDAN, R. P., KARNACHI, P., TUDOR, M., XU, Y., LIAW, A., SHAH, F., CHENG, A. C., JOSHI, E., GLICK, M., AND ALVAREZ, J. Experimental error, kurtosis, activity cliffs, and methodology: What limits the predictivity of quantitative Structure-Activity relationship models? *J Chem Inf Model* 60, 4 (Apr. 2020), 1969–1982.
- [33] STERLING, T., AND IRWIN, J. J. Zinc 15 – ligand discovery for everyone. *Journal of Chemical Information and Modeling* 55, 11 (2015), 2324–2337. PMID: 26479676.
- [34] STEVENS, K. L., RENO, M. J., ALBERTI, J. B., PRICE, D. J., KANE-CARSON, L. S., KNICK, V. B., SHEWCHUK, L. M., HASSELL, A. M., VEAL, J. M., DAVIS, S. T., ET AL. Synthesis and evaluation of pyrazolo [1, 5-b] pyridazines as selective cyclin dependent kinase inhibitors. *Bioorganic & medicinal chemistry letters* 18, 21 (2008), 5758–5762.
- [35] STUMPFE, D., HU, Y., DIMOVA, D., AND BAJORATH, J. Recent progress in understanding activity cliffs and their utility in medicinal chemistry. *Journal of Medicinal Chemistry* 57, 1 (2014), 18–28. PMID: 23981118.

- [36] SUN, R., DAI, H., AND YU, A. W. Does gnn pretraining help molecular representation? In *Advances in Neural Information Processing Systems* (2022), S. Koyejo, S. Mohamed, A. Agarwal, D. Belgrave, K. Cho, and A. Oh, Eds., vol. 35, Curran Associates, Inc., pp. 12096–12109.
- [37] TAVARES, F. X., BOUCHERON, J. A., DICKERSON, S. H., GRIFFIN, R. J., PREUGSCHAT, F., THOMSON, S. A., WANG, T. Y., AND ZHOU, H.-Q. N-phenyl-4-pyrazolo [1, 5-b] pyridazin-3-ylpyrimidin-2-amines as potent and selective inhibitors of glycogen synthase kinase 3 with good cellular efficacy. *Journal of medicinal chemistry* 47, 19 (2004), 4716–4730.
- [38] TROTT, O., AND OLSON, A. J. Autodock vina: improving the speed and accuracy of docking with a new scoring function, efficient optimization, and multithreading. *Journal of computational chemistry* 31, 2 (2010), 455–461.
- [39] VAN DER MAATEN, L., AND HINTON, G. Visualizing data using t-sne. *Journal of Machine Learning Research* 9, 86 (2008), 2579–2605.
- [40] VAN TILBORG, D., ALENICHEVA, A., AND GRISONI, F. Exposing the limitations of molecular machine learning with activity cliffs. *Journal of Chemical Information and Modeling* 62, 23 (dec 2022), 5938–5951.
- [41] VELIČKOVIĆ, P., FEDUS, W., HAMILTON, W. L., LIÒ, P., BENGIO, Y., AND HJELM, R. D. Deep graph infomax. In *International Conference on Learning Representations* (2019).
- [42] WANG, Y., WANG, J., CAO, Z., AND BARATI FARIMANI, A. Molecular contrastive learning of representations via graph neural networks. *Nature Machine Intelligence* 4, 3 (Mar. 2022), 279–287.
- [43] WANG, Z., ZHANG, Q., HU, S.-W., YU, H., JIN, X., GONG, Z., AND CHEN, H. Multi-level Protein Structure Pre-training via Prompt Learning. In *The Eleventh International Conference on Learning Representations* (2023).
- [44] WEININGER, D. Smiles, a chemical language and information system. 1. introduction to methodology and encoding rules. *Journal of Chemical Information and Computer Sciences* 28, 1 (1988), 31–36.
- [45] WU, F., QIN, H., LI, S., LI, S. Z., ZHAN, X., AND XU, J. Instructbio: A large-scale semi-supervised learning paradigm for biochemical problems, 2023.
- [46] WU, Z., RAMSUNDAR, B., FEINBERG, E., GOMES, J., GENIESSE, C., PAPPU, A. S., LESWING, K., AND PANDE, V. Moleculenet: a benchmark for molecular machine learning. *Chem. Sci.* 9 (2018), 513–530.
- [47] XIA, J., ZHAO, C., HU, B., GAO, Z., TAN, C., LIU, Y., LI, S., AND LI, S. Z. Mole-BERT: Rethinking pre-training graph neural networks for molecules. In *The Eleventh International Conference on Learning Representations* (2023).
- [48] XU, D., CHENG, W., LUO, D., CHEN, H., AND ZHANG, X. Infogcl: Information-aware graph contrastive learning. In *Advances in Neural Information Processing Systems* (2021), M. Ranzato, A. Beygelzimer, Y. Dauphin, P. Liang, and J. W. Vaughan, Eds., vol. 34, Curran Associates, Inc., pp. 30414–30425.
- [49] XU, K., HU, W., LESKOVEC, J., AND JEGELKA, S. How powerful are graph neural networks? In *International Conference on Learning Representations* (2019).
- [50] XU, M., WANG, H., NI, B., GUO, H., AND TANG, J. Self-supervised graph-level representation learning with local and global structure. In *Proceedings of the 38th International Conference on Machine Learning* (18–24 Jul 2021), M. Meila and T. Zhang, Eds., vol. 139 of *Proceedings of Machine Learning Research*, PMLR, pp. 11548–11558.
- [51] YING, Z., BOURGEOIS, D., YOU, J., ZITNIK, M., AND LESKOVEC, J. Gnnexplainer: Generating explanations for graph neural networks. In *Advances in Neural Information Processing Systems* (2019), H. Wallach, H. Larochelle, A. Beygelzimer, F. d'Alché-Buc, E. Fox, and R. Garnett, Eds., vol. 32, Curran Associates, Inc.

- [52] YING, Z., YOU, J., MORRIS, C., REN, X., HAMILTON, W., AND LESKOVEC, J. Hierarchical Graph Representation Learning with Differentiable Pooling.
- [53] YOU, Y., CHEN, T., SHEN, Y., AND WANG, Z. Graph Contrastive Learning Automated.
- [54] ZHANG, Z., BIAN, Y., XIE, A., HAN, P., HUANG, L.-K., AND ZHOU, S. Can pre-trained models really learn better molecular representations for ai-aided drug discovery?, 2022.
- [55] ZHU, Y., XU, Y., YU, F., LIU, Q., WU, S., AND WANG, L. Graph contrastive learning with adaptive augmentation. In *Proceedings of the Web Conference 2021* (New York, NY, USA, 2021), WWW '21, Association for Computing Machinery, p. 2069–2080.

Supplementary Information of From molecules to scaffolds to functional groups: building context-dependent molecular representation via multi-channel learning

Yue Wan¹, Jialu Wu², Tingjun Hou^{2*}, Chang-Yu Hsieh^{2*}, Xiaowei Jia^{1*}
*University of Pittsburgh, Computer Science Department, Pittsburgh, PA 15260, United States*¹
*Innovation Institute for Artificial Intelligence in Medicine of Zhejiang University,
College of Pharmaceutical Sciences, Zhejiang University, Hangzhou, 310058, China*²

1 Similarity comparison

We compare the relationship between the conventional fingerprint/descriptor similarity measures and the learned representation distances across channels (i.e., [MCD], [SCD], and [CP]), we randomly sample 1000 molecule pairs from ZINC15 [5] and examine the correlation between the conventional molecule similarity measures and the learned representation distances. To be more specific, we compute the tanimoto similarity between molecule Morgan fingerprints [3], scaffold Morgan fingerprints, and functional groups (i.e., motif) descriptors [4]. We compute and normalize the L2 norm distance between the learned representations. As shown in Figure S1, the representation distance is highly correlated with the conventional similarity measures. This alignment also confirms that the representations learned from different channels indeed capture different global-local perspectives of the molecule.

2 Implicit representation hierarchy

As previously discussed, the representations learned via different channels can elicit different levels of global and local molecule attributes. Molecule distancing focuses on the global view of the molecule, scaffold distancing targets the partial view, and context prediction tackles the local view (i.e., functional groups composition). To better visualize this representation hierarchy, we perform an iterative clustering analysis over the molecule space of the ChEMBL237 dataset. Specifically, we conduct three stages of clustering with respect to the three channeled representations. Each stage considers the clustered results from the previous stage and further refines the clustered subspace. In hypothesis, representations derived from context prediction (i.e., $h_g^{[CP]}$) may result in a coarse-grained clustering in terms of the intra-cluster molecule similarity. This is because molecules with identical functional groups can still elicit structural differences. In comparison, representations from scaffold distancing (i.e., $h_g^{[SCD]}$) could yield a less coarse-grained clustering by grouping molecules with similar scaffolds together. Representations from molecule distancing (i.e., $h_g^{[MCD]}$) consider structural variations beyond the scaffold, potentially leading to a more fine-grained clustering.

*Corresponding authors.

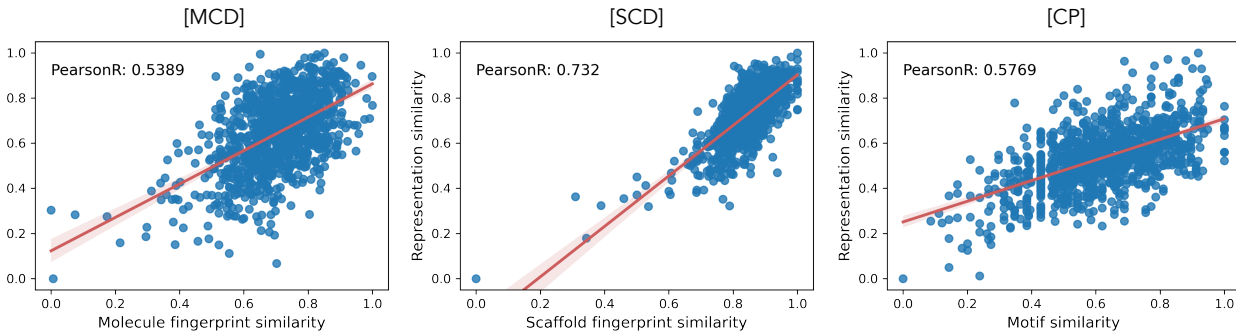


Figure S1: **Comparison of conventional similarity measures and representation distance.** For illustration purpose, 1000 molecule pairs are randomly sampled from ZINC15. The x-axis represents the conventional molecule similarity, while the y-axis represents the normalized L2 norm between representations. Pearson correlation coefficient is reported.

As shown in Figure S2, we first perform clustering with $h_g^{[CP]}$. The bar chart illustrates the normalized ratio of intra-cluster motif distance to inter-cluster motif distance from the top-10 largest clusters. It suggests that intra-cluster molecules are more likely to have similar functional groups composition. Peeking inside the clusters, examples show the shared set of functional groups among the grouped molecules, which is denoted as the cluster tag. The two numbers at the x-axis represent the number of unique scaffolds and the cluster size, respectively. It means that the grouped molecules at this stage are not necessarily structurally similar. We further perform the stage two clustering using $h_g^{[SCP]}$ on top of the stage 1 results. Again, the bar chart (with darker color) illustrates the normalized ratio of intra-cluster scaffold distance to inter-cluster scaffold distance. Five out of ten clusters contain molecules with same scaffolds. At stage three, the molecule space are further refined using representation $h_g^{[MCP]}$. Despite the grouped molecules from stage two already share common scaffolds, the representation could still capture the minor structural differences in the terminal side chains as shown by the examples. From coarse-grained to fine-grained, the cluster becomes increasingly refined after iteratively applying clustering along the multi-channeled representations. It supports the hypothesis that representations from different channels can capture different views of the molecules from global to local.

3 Roughness comparison

In this section, we report the roughness index (ROGI) [1] difference between our method and two SSL baseline methods (GraphLoG, MolCLR) prior to finetuning on 33 datasets. We also consider the Morgan Fingerprint (MorganFP) [3] as one of the traditional molecule representations used in machine learning. The ROGI value captures the roughness of the property landscape given a representation. Low ROGI value indicates better modellability, and is strongly correlated with the convergence rate and the overall performance at the finetune stage. As shown in Figure S4, our representation has better ROGI value compared to other deep molecule representations in 22 out of 33 datasets. Its ROGI value is also lower than that of MorganFP in 18 out of 33 datasets. The advantage of the fingerprint representations is consistent with the finding in [9]. However, it does not guarantee that the finetuning performance using fingerprints must outperform other deep learning

E-mail addresses: tingjunhou@zju.edu.cn (T. Hou), kimhsieh@zju.edu.cn (C.-Y. Hsieh), xiaowei@pitt.edu (X. Jia)

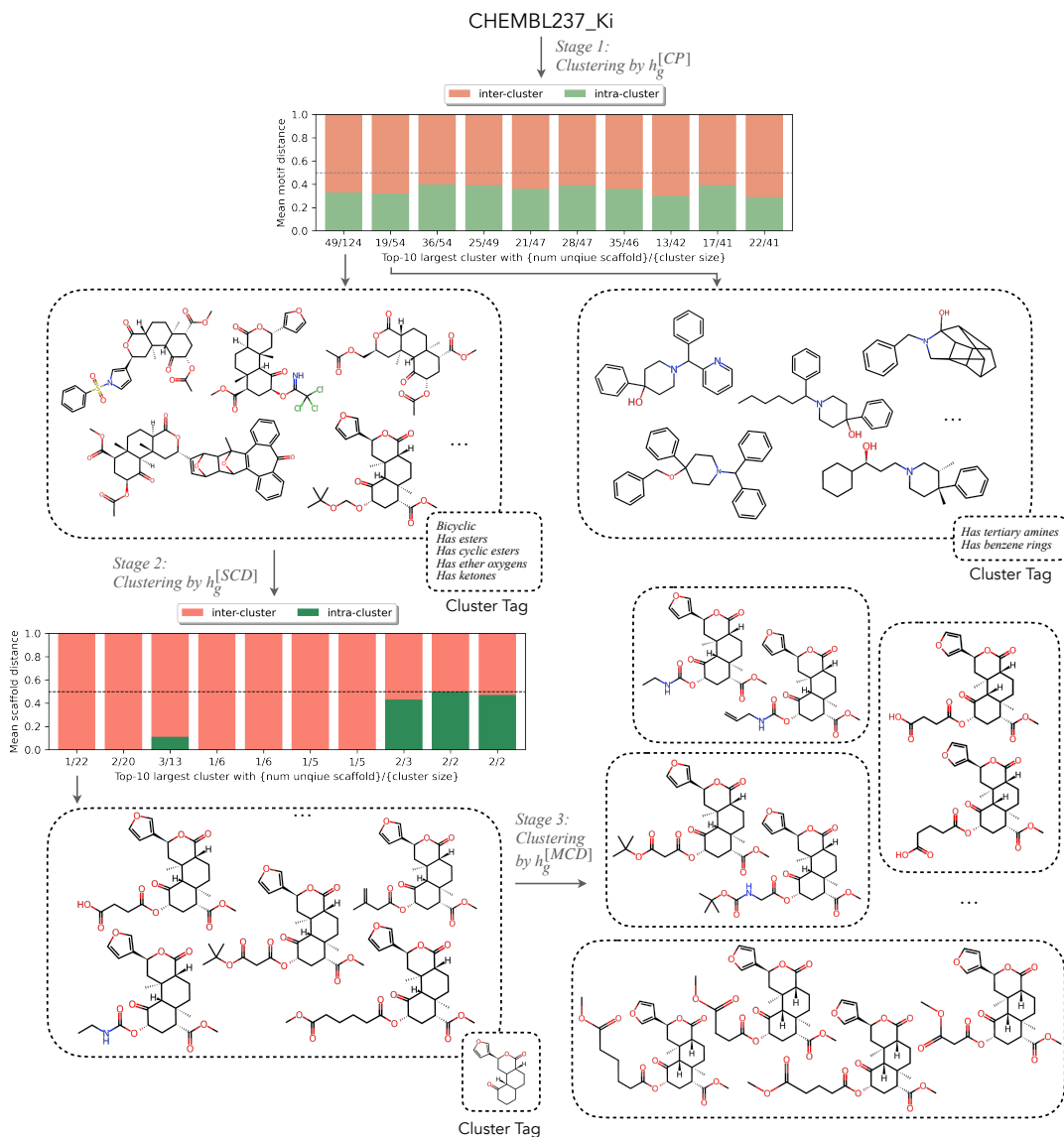


Figure S2: Hierarchical clustering supported by the multi-channel representation.

methods. This is because the pretrained molecule representations serve only as initialization for the embedding space. The model parameters, which are responsible for outputting these representations, also undergo parameter updates during the finetuning optimization process. In other words, the updated representations continue to benefit from the flexibility and strength of deep learning models.

4 Convergence rate

We present a comparative analysis of the downstream convergence rates among our proposed method, GraphLoG, and MolCLR in four example datasets (CHEMBL237_Ki, CHEMBL262_Ki, CHEMBL2034_Ki, and CHEMBL234_Ki). As illustrated in the Figure S5, our representation facilitates faster convergence rate in terms of both the training and validation R-squared value. It suggests that our representation exhibits better downstream transferability, which is consistent with the conclusions on modellability discussed in Section 3 in the main text. To further understand

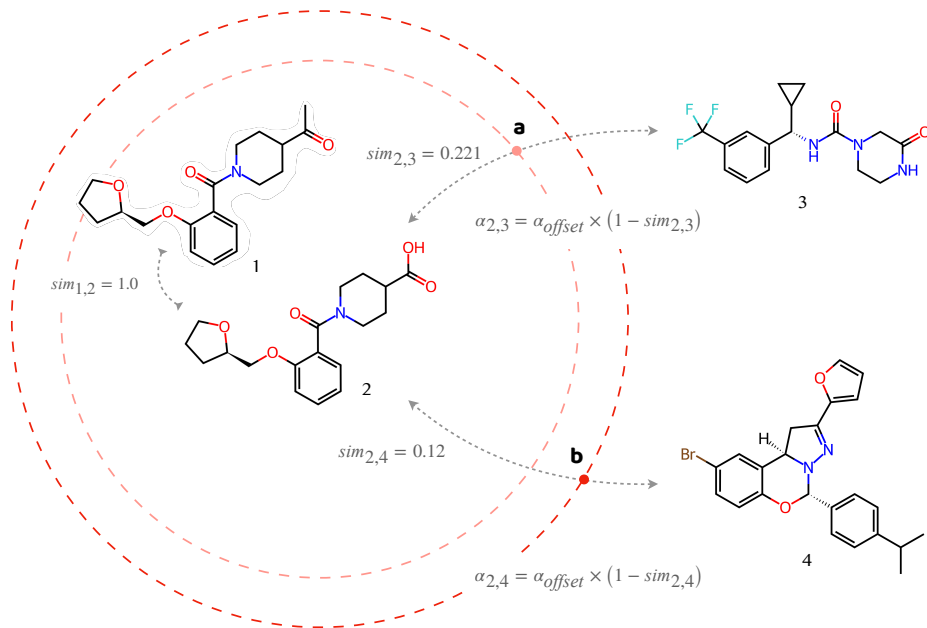


Figure S3: **Adaptive margin loss.** Triplet examples $\langle 1, 2, 3 \rangle$ and $\langle 1, 2, 4 \rangle$ considered in scaffold distancing adaptive margin loss. $sim_{i,j}$ represents the scaffold fingerprint tanimoto similarity between compound i and j , while $\alpha_{i,j}$ corresponds to the computed margin (indicated by the dashed line). Note that, in this example, (a) the margin $\alpha_{2,3}$ is smaller than (b) the margin $\alpha_{2,4}$ because of the similarity difference. Both compound 3 and 4 lie outside of the margin, hence making the triplet loss $\ell_{1,2,3} = \ell_{1,2,4} = 0$. However, the actual representation distance between $\langle 2, 3 \rangle$ and $\langle 2, 4 \rangle$ may not necessarily correlate with the computed margins, as shown by the figure. This motivates our quadruplets formulation.

the efficacy of our composite representation achieved through prompt weight selection, we also consider the downstream performance when solely finetuned from individual channels, represented by *ours_mcd*, *ours_scd*, and *ours_cp*. A notable observation is that their performance often exhibits high volatility, such that both the training and validation R-squared value oscillates significantly between epochs. One plausible explanation is that each corresponded prompt-guided aggregation module considers atoms with varying degrees of importance. In other words, individual aggregations may only tackle a partial view of the molecule, especially for the [SCD] and [CP] channels. Given that the aggregation modules remain fixed during finetuning, these partial perspectives may fall short in comprehensively learning the structure-property relationship.

5 Representation robustness

In the main text, we evaluate the shift in representation space with three methods (Ours, MolCLR [7], and GraphLoG [8]) when finetuned on the ChEMBL237_Ki dataset. In this section, we further analyze the representation performance under the few-shot scenarios. Specifically, we evaluate the finetuned results of the validation set using only 1%, 5%, 10%, 50%, and 100% of the training data, corresponding to the 1-shot, 5-shot, 10-shot, 50-shot, 100-shot columns as shown in Figure S6. Following the work in [6], instead of randomly sampling the training data, we perform stratified sampling by first applying KMeans clustering using the molecule fingerprint, and selecting the

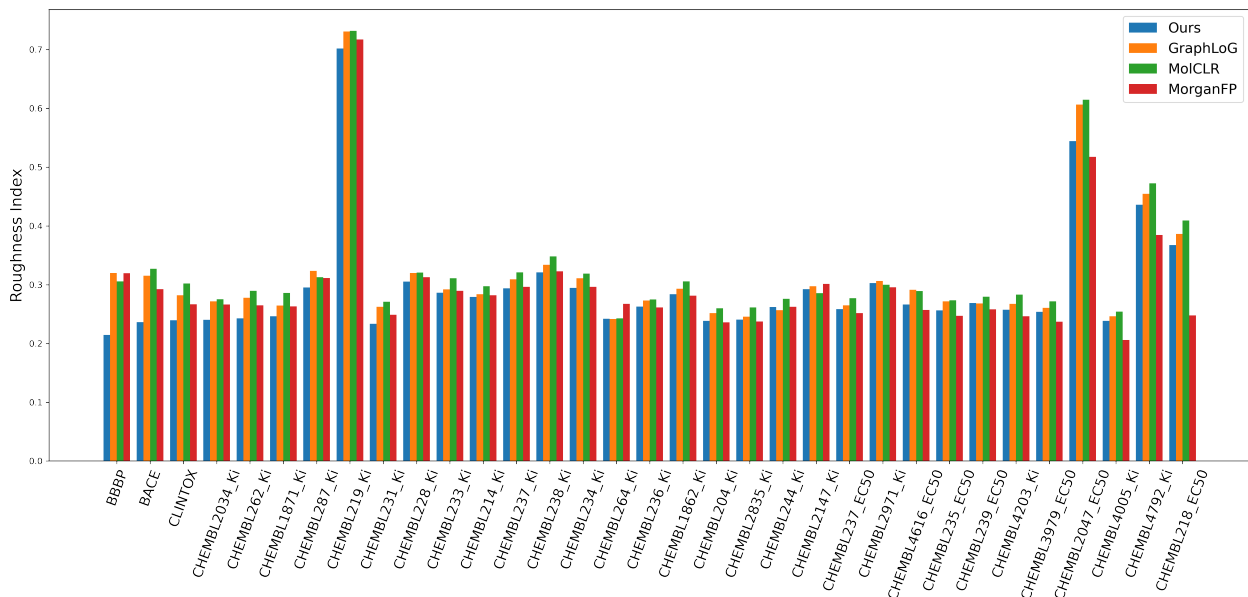


Figure S4: **Roughness index (ROGI) comparison.** The computed ROGI value of the representations (Ours, GraphLoG, MolCLR, and Morgan Fingerprint) against molecular property measures in 33 datasets. The bars are arranged from left to right based on the descending order of the ROGI value differences between our representation and the most effective alternative representation.

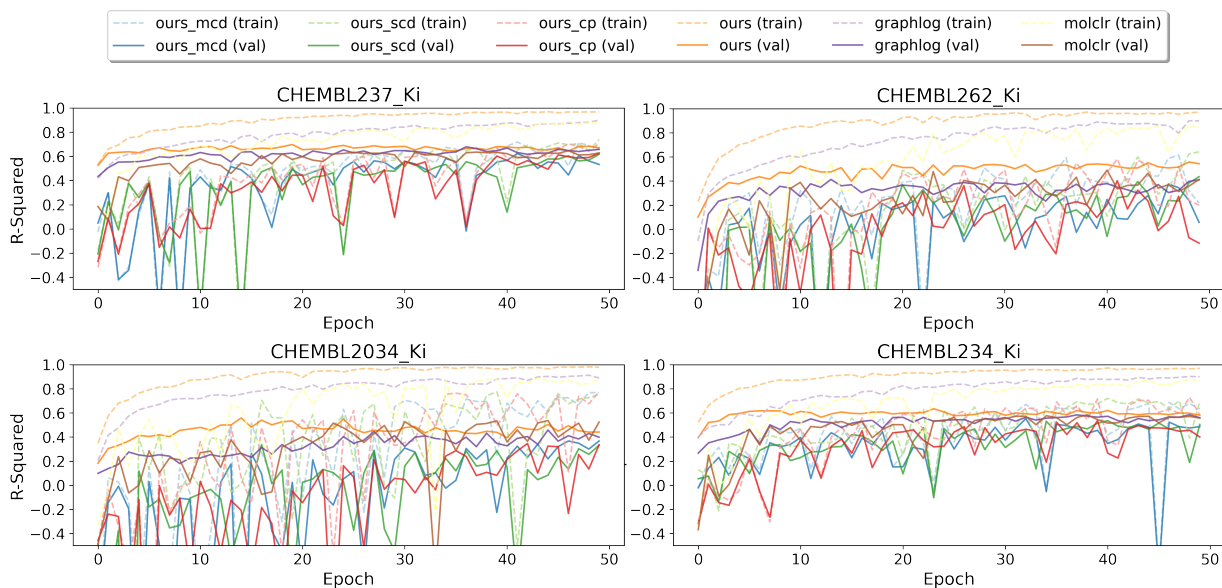


Figure S5: **Convergence rate at finetuning.** R-squared curves of both training and validation set from four datasets are plotted. The dashed line represents the training R-squared value, while the solid line corresponds to the validation r-squared value.

required amount of data samples that are diverse across the clustering. We report the same Rand index [2] and cliff-noncliff distance ratio as the analysis in the main text. As shown in the figure, even with 1% of training data, the representation space of MolCLR distorts significantly. The small

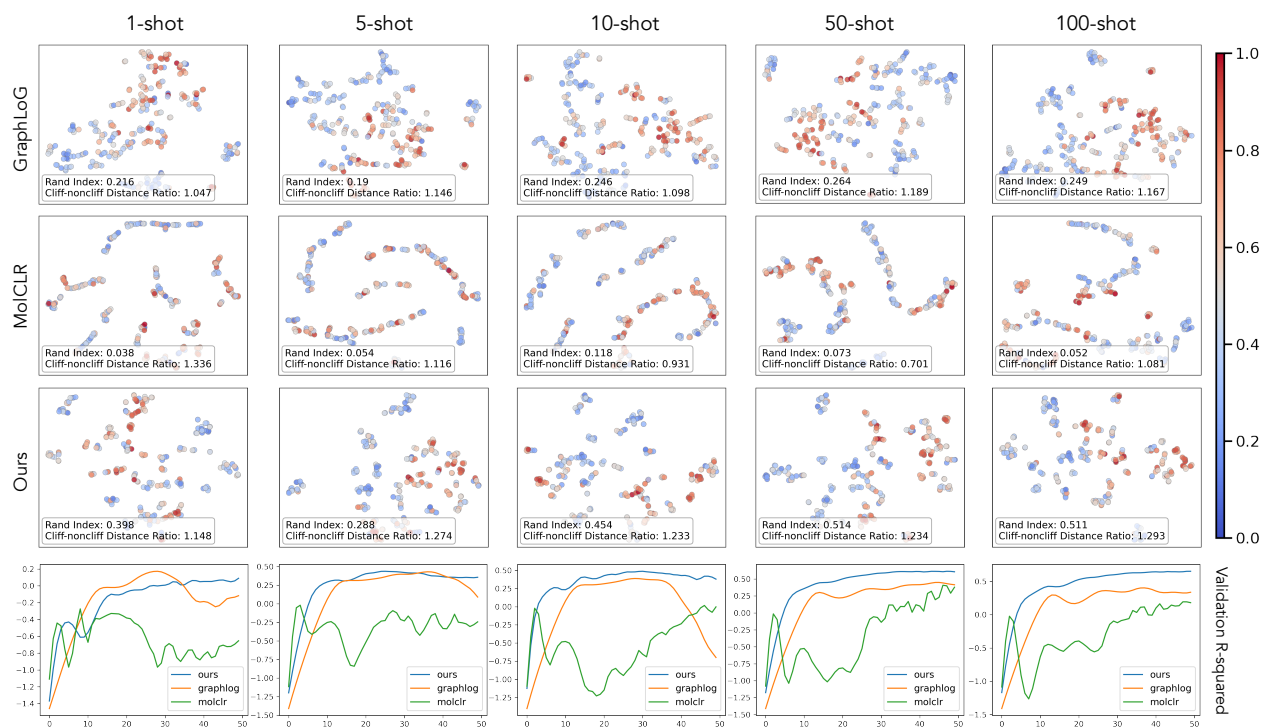


Figure S6: **Representation space probing (few-shot scenario)**. The dynamics of molecule representation space of three methods of five few-shot settings on dataset CHEMBL237_Ki. For each row pair, a 2-D view of the representation space of the validation set is visualized. The dot coloring represents the normalized potency labels. Rand index and cliff-noncliff distance ratio are reported, along with the validation r-squared value along the training process (bottom row).

rand index implies that large amount of structural information is lost, which can also be interpreted as label overfitting. GraphLoG, compared to MolCLR, shows a more balanced representation space mapping throughout all few-shot scenarios, also indicated by its consistently stable rand index around 0.24. Our method also maintains high Rand index across all few-shot scenarios. When comparing the cliff-noncliff distance ratio, our method consistently performs better than others with larger distance ratio. As shown by the validation r-squared curves, our method also achieves better performance in terms of the highest r-squared value, faster convergence rate, and training stability.

References

- [1] ALDEGHI, M., GRAFF, D. E., FREY, N., MORRONE, J. A., PYZER-KNAPP, E. O., JORDAN, K. E., AND COLEY, C. W. Roughness of Molecular Property Landscapes and Its Impact on Modellability. *Journal of Chemical Information and Modeling* 62, 19 (Oct. 2022), 4660–4671.
- [2] HUBERT, L., AND ARABIE, P. Comparing partitions. *Journal of Classification* 2, 1 (Dec 1985), 193–218.
- [3] MORGAN, H. L. The generation of a unique machine description for chemical structures—a technique developed at chemical abstracts service. *Journal of Chemical Documentation* 5, 2 (1965), 107–113.
- [4] RONG, Y., BIAN, Y., XU, T., XIE, W., WEI, Y., HUANG, W., AND HUANG, J. Self-Supervised Graph Transformer on Large-Scale Molecular Data.
- [5] STERLING, T., AND IRWIN, J. J. Zinc 15 – ligand discovery for everyone. *Journal of Chemical Information and Modeling* 55, 11 (2015), 2324–2337. PMID: 26479676.
- [6] VAN TILBORG, D., ALENICHEVA, A., AND GRISONI, F. Exposing the limitations of molecular machine learning with activity cliffs. *Journal of Chemical Information and Modeling* 62, 23 (dec 2022), 5938–5951.
- [7] WANG, Y., WANG, J., CAO, Z., AND BARATI FARIMANI, A. Molecular contrastive learning of representations via graph neural networks. *Nature Machine Intelligence* 4, 3 (Mar. 2022), 279–287.
- [8] XU, M., WANG, H., NI, B., GUO, H., AND TANG, J. Self-supervised graph-level representation learning with local and global structure. In *Proceedings of the 38th International Conference on Machine Learning* (18–24 Jul 2021), M. Meila and T. Zhang, Eds., vol. 139 of *Proceedings of Machine Learning Research*, PMLR, pp. 11548–11558.
- [9] ZHANG, Z., BIAN, Y., XIE, A., HAN, P., HUANG, L.-K., AND ZHOU, S. Can Pre-trained Models Really Learn Better Molecular Representations for AI-aided Drug Discovery?, Aug. 2022. arXiv:2209.07423 [cs, q-bio].